ANNALI DI GEOFISICA, VOL. XXXVII, N. 3, June 1994

Near real time estimation of magnitudes and moments for local seismic events

Cenk Deniz Mendi ([1])([2]) **and Eystein S. Husebye** ([1])
([1]) *University of Bergen, Institute of Solid Earth Sciences, Bergen, Norway*
([2]) *On leave from TÜBİTAK, Marmara Research Center, Earth Sciences Department, Gebze, Kocaeli, Turkey*

Abstract
The general popularity of magnitude as a convenient and robust measure of earthquake size makes it tempting to examine whether this parameter can be reliably estimated in near real time. In this study we demonstrate that this is indeed the case conditioned on the design of the signal detector being of STA/LTA type where STA is a short term signal power or rms estimate. Using real data we demonstrate the Random Vibration Theory relation that $A_{max} \sim (2\ln N)^{1/2} A_{rms}$ is valid for non-stationary seismic signals. Using Rayleigh's theorem we also established a relation between A_{rms} and the flat portion of the source spectra. These A_{max} and A_{rms} estimation procedures are used for determining conventional magnitudes and moment magnitudes for 29 events as recorded by the Norwegian Seismograph Network (NSN). We used here a procedure outlined by Sereno *et al.* (1988) and also their geometrical spreading and attenuation parameters derived from analysis of NORSAR recordings. Our magnitude and moment magnitude estimates for 5 different frequency bands are in good agreement with the M_L estimates derived from the conventional magnitude formulas in combination with empirical correction tables. Surprisingly, the A_{max} and A_{rms} magnitudes produced consistent negative biased by ca. 0.4 units estimates even in the extreme 4-8 Hz band. In view of the good agreement between various types of magnitude estimates, we constructed conventional magnitude correction tables spreading and attenuation parameters from Sereno *et al.* (1988) for a variety of signal frequency bands. Near real time A_{max} ad/or A_{rms} or correspondingly event magnitudes would be of significance in automatic phase association analysis, bulletin production for local and regional seismic networks and the earthquakes monitoring performances of such networks.

Key words *random vibration theory – distance corrections – spreading and attenuation effects – network monitoring – capabilities in real time*

1. Introduction

The concept of earthquake magnitude was firstly introduced by Richter (1935). He proposed a logarithmic amplitude scale tied to the first arriving P wave as a measure for the relative size of local Southern California earthquakes. This simple and robust magnitude scale being popular with seismologists around the world, it has been extended to all distance ranges and many seismic phases (Nuttli, 1973; Båth *et al.*, 1981; Ebel, 1982). Despite the diversity of record measurements, tied to the maximum amplitudes of P, S and surface waves, all such scales are of similar forms

$$M = \log\left(\frac{A}{T}\right) + q(r,f) + c \qquad (1.1)$$

where M is the magnitude, A the maximum phase amplitude, T is the period (s), q ac-

counts for geometrical spreading and attenuation as a function of distance r (km) and signal frequency (f) while c is a station correction term. Focal depth (h) is seldom included explicitly in magnitude formulas although it is significant in case of surface waves from deep events.

Although an occurring earthquake is a complex phenomenon, the Richter magnitude remains highly useful in many seismological contexts. A drawback with such measurement using conventional instrumentation is that earthquake phase amplitudes may be measured at frequencies beyond the corner frequency of the source spectra which cause a consistent magnitude bias. Therefore, many seismologists argue in favour of replacing magnitude with Aki's (1967) earthquake moment M_0 which may be obtained from inversion of broadband waveform data (Dziewonski and Gilbert, 1974; Jost and Herrmann, 1989) or equivalently the level of the flat portion of the source spectra. To avoid confusion, moment-magnitude scales have been introduced in the form of linear relationships between the moment (M_0) and magnitude. For example, Sereno *et al.* (1988) introduced the following formula for local Scandinavian earthquakes:

$$\log (M_0) = 1.03M_L + 17.1 \quad (1.2)$$

where M_L is the local L_g magnitude.

In eq. (1.1) the A/T measurement remains essentially a manual operation while the q-term is derived from empirical tables when an epicenter solution is at the hand. In this paper we address the problem of undertaking in near real time event magnitude and/or moment measurements. This study is tied to analysis of local events because M_L-magnitude estimation is often problematic due to complex geometrical spreading and attenuation relationships at small distance ranges. It is considered an important task in view of the widespread use of event magnitude in observational seismology and the potential of using amplitude information in automatic schemes for epicenter location (Ruud *et al.*, 1993; Sambridge and Gallagher, 1993) and network performance simulations (Sereno *et al.*, 1988).

2. On line A/T estimation

Obviously for near real time magnitude/moment estimation, the A/T term must be an integral part of the signal detector design. The most popular ones in use are the so-called sliding window STA/LTA type which is a comparison of short and long term trace amplitude (a_i) averages (*e.g.*, Ruud and Husebye, 1992). Common STA definitions are of the forms:

$$\text{STA (abs)} = \frac{1}{n} \sum_{i=1}^{n} | a_i | \quad (2.1)$$

$$\text{STA (rms)} = \left[\frac{1}{n} \sum_{i=1}^{n} a_i^2 \right]^{1/2} \quad (2.2)$$

Equivalent expressions are valid for LTA when the effective window length n is increased 10-20 times that of the STA window length. The STA and LTA terms are commonly measured in near real time on bandpass filtered seismometer output traces. When the STA/LTA ratio exceeds a present threshold, the presence of a seismic signal is declared. Our preference is for the rms related STA-LTA definitions also because signal rms is related to the signal power spectrum via the Parseval's theorem.

From eq. (2.2) the task is to estimate peak time domain amplitudes for the first arrival of P-waves or the dominant L_g-phase in case of local events that is the A/T-term in eq. (1.1). From the Random Vibration Theory (RVT) results of Cartwright and Longuet-Higgins (1956) we have the relation

$$E(A_{\max}) = A_{\text{rms}} f(N) \quad (2.3)$$

where E is expectation, N is the number of

extremes (peaks and troughs) and A_{rms} is the rms value of the signal. In the case of STA trace window, A_{rms} = STA(rms). We have for $f(N)$

$$f(N) = (2\ln N)^{1/2} \qquad (2.4)$$

The RVT assumes stationary time series (Crandal and Mark, 1963) which are seldom the case for seismic recordings. However, Boore (1983) and Boore and Joyner (1984) have demonstrated that the RVT relation in eq. (2.3) performs well even in cases of peak signal accelerations and velocities as determined from time domain simulations. The validity of the simple linear relationship in eq. (2.3) was confirmed by extensive analysis of real data, and such results are detailed in the data analysis section.

Whether we prefer to measure magnitude (M_L) or moment (M_0), the A_{max} term is estimated from bandpass filtered traces, and thus must be corrected for the instrument response. A reasonable assumption here is that the displacement response spectra are approximately flat within the filter passband, and that the instrument response correction is tied to the center frequency of the bandpass filter. Similarly, the period (T) of the maximum signal amplitude is also tied to the center frequency of the bandpass filter. Thus, both the A_{max} and T terms in magnitude formula (eq. (1.1)) are obtained via eq. (2.3).

3. Magnitude measurements

The A/T-term derived via the detector parameter STA(rms) is sufficient for event magnitude estimation given that a tabulation of the distance dependent q-term in eq. (1.1) is available. However, for many regions the q-term is not well known at local and regional distances making corresponding event magnitude estimates unreliable. For example, as a rule the ISC does not estimate P-wave magnitudes for $r < 20°$. In other cases, available correction tables were derived from old analog recordings in the 1-2 Hz bandpass while modern instrument recordings of local events are dominated by 3-6 Hz signal frequencies. An additional problem is that intraplate seismicity levels are so low that it is difficult to calibrate the local event magnitudes towards those obtained from teleseismic recordings.

In other words, local magnitude scales may differ significantly from each other, so recently seismologists have been exploring the usefulness of event moment magnitude scales.

3.1. *Moment measurements*

As mentioned above, the q-term in eq. (1.1) is not always well established, and a way of circumventing this problem is to introduce specific estimates of the geometrical spreading and attenuation (Q) effects. Following Sereno *et al.* (1988), we write for the amplitude spectrum of displacement at epicenter distance r

$$| A(f, r) | = S(f)G(r, r_0) \exp\left[\frac{-\pi f t}{Q(f)}\right] \qquad (3.1)$$

where f is frequency, $S(f)$ source spectra, $G(r, r_0)$ geometrical spreading function with a reference distance (r_0), and $Q(f)$ the attenuation function. The attenuation function is of the form

$$Q(f) = Q_0 f^{\gamma} \qquad (3.2)$$

where the frequency dependence is through the f^{γ} expression. The geometrical spreading term is of the form

$$G(r, r_0) = \begin{cases} (1/r)^{\mu} & ; \ r \le r_0 \\ (1/r_0)(r_0/r)^{\nu} & ; \ r \ge r_0 \end{cases} \qquad (3.3)$$

where the r_0, μ, and ν parameters depend on the phase type and besides may vary from one tectonic regime to another. At lo-

cal distances the dominant signal in the records is the L_g-phase whose source spectrum in case of an earthquake is expressed as (Sereno *et al.*, 1989)

$$S(f) = S_0 H(f, f_c) \tag{3.4}$$

$$H(f, f_c) = \left(1 + (1 - 2B)\left(\frac{f}{f_c}\right)^2 + B^2\left(\frac{f}{f_c}\right)^4\right)^{-1/2} \tag{3.5}$$

where S_0 is the low frequency spectral source level, f_c is the corner frequency of the source spectrum, B is the amount of overshoot (Xie, 1993). We have the following relations for f_c and S_0 regarding M_0:

$$f_c = cS_0^{-1/3}; \qquad S_0 = \frac{M_0}{4\pi\varrho\beta^3} \tag{3.6}$$

where β is the crustal shear wave velocity, ϱ the crustal density and c a scaling constant. For moment/magnitude estimation, we must establish a relationship between the amplitude spectrum of the displacement ($| A(f, r) |$) and the near «real-time» record parameters, A_{rms} or A_{max}, namely

$$| A(f_{0i}, r) | = \sqrt{\frac{\Delta T}{2\Delta f_i}} A_{\text{rms}}; \qquad i = 1,...,5 \tag{3.7}$$

$$| A(f_{0i}, r) | \cong \frac{1}{2\Delta f_i} A_{\text{max}} \qquad ; \qquad i = 1,...,5 \tag{3.8}$$

where f_{0i} represents the center frequencies of the 5 bandpass filters used in data analysis, $| A(f_{0i}, r) |$ is the amplitude spectrum at frequency f_{0i} and distance r, ΔT is the window length in s and Δf_i is the bandwidth of the i^{th} filter. The derivations of eq. (3.7) and eq. (3.8) are detailed in Appendix.

The source spectrum decays with f^{-2} beyond the f_c due to the H function. From eq. (3.6) we can estimate the S_0 and f_c parameters. However, in practice the corner frequency is not well resolved, so our preference was to fix it at a «safe» value of 20 Hz which is also very close to the bandwidth of the signals used in analysis (sampling frequency = 50 Hz). Under this assumption, the $H(f, f_c)$ is negligible and combining eqs. (3.1), (3.6), (3.7) and (3.8) we get

$$\log M_{0(\text{max})} \cong \cong \log A_{\text{max}} - \log 2\Delta f_i + \log 4\pi\varrho\beta^3 + - \log G(r, r_0) + \frac{\pi f t}{Q(f)} \log e \tag{3.9}$$

$$\log M_{0(\text{rms})} = = \log A_{\text{rms}} + \frac{1}{2} \log \frac{\Delta T}{2\Delta f_i} + \log 4\pi\varrho\beta^3 + - \log G(r, r_0) + \frac{\pi f t}{Q(f)} \log e \tag{3.10}$$

Note that P, S and L_g-phases from explosions and earthquakes respectively have different source representations. However, the main point is that it should be feasible to estimate in near real time event magnitude and event moment from «real-time» available signal detector parameters. The validity of this statement will be demonstrated in the next section.

4. Data analysis and results

In this section we would demonstrate that the deduced $A_{\text{max}} - A_{\text{rms}}$ relationship in eq. (2.3) appears to be valid for the recordings of local earthquakes and explosions at stations equipped with short period seismometers. We use observations from the Norwegian Seismograph Network (NSN) whose station locations are shown in fig. 1. A more subtle but extensive test was performed by calculat-

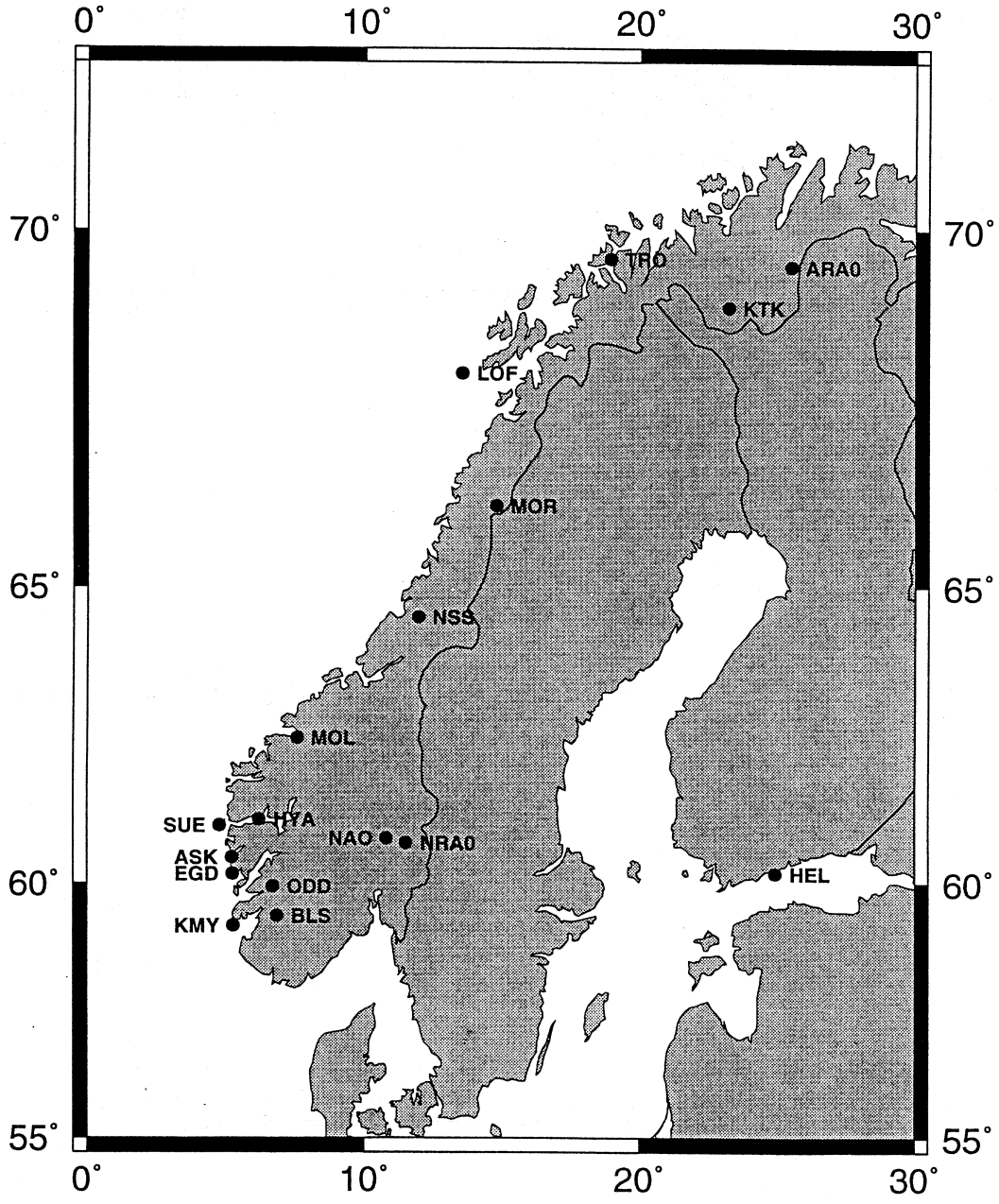

Fig. 1. Stations constituting the Norwegian Seismograph Network (NSN) which is operated by the University of Bergen. Some of the stations are equipped with three-component instrumentation. In our analysis only the vertical short period recordings are used. The NORSAR operated regional arrays NORESS (NAO, NRA0) and ARCESS (ARA0) are also marked.

Table I. Listing of all the events used in our analysis. The focal parameters are taken from the monthly bulletins for the Norwegian Seismic Network (NSN) as published by the University of Bergen. The M_c and M_L notations reflect NSN coda wave magnitude and NORSAR reported M_L (L_g-waves) magnitude, respectively. We have introduced a few modifications in parameter listing; all presumed explosions (EXP) are given zero focal depth. The separation of events into EXP and EQ (earthquake) populations are not based on specific classification criteria. Potential errors here would not significantly change our analysis results.

N.	Date	Time	Location		M_c	M_L	H	#	Source
	(d/m/y)	(h.min:s)	(LatN)	(LonE)			(km)	Stat.	type
1	26/08/93	10.34:32.0	59.05	5.77	2.6	2.2	0	8	EXP
2	26/08/93	19.22:04.9	61.11	4.07	2.8	2.5	18	8	EQ
3	10/09/93	13.11:23.8	58.34	6.36	2.7	2.0	0	5	EXP
4	13/09/93	05.25:14.4	66.34	5.67	3.9	3.2	11	10	EQ
5	15/09/93	09.58:38.1	60.60	4.79	2.1	1.6	0	7	EXP
6	15/09/93	15.31:29.7	67.11	20.84	3.2	1.8	0	4	EXP
7	21/09/93	13.15:21.1	58.33	6.31	3.0	2.5	0	7	EXP
8	28/09/93	16.44:53.9	58.49	10.62	2.9	2.3	15	5	EQ
9	28/09/93	16.57:42.1	60.46	5.15	1.6	1.4	0	6	EXP
10	29/09/93	14.12:21.5	58.15	6.31	2.8	2.2	0	6	EXP
11	02/10/93	08.30:55.3	60.39	5.02	1.8	1.5	0	6	EXP
12	03/10/93	23.48:35.5	60.06	7.29	2.5	1.8	15	7	EQ
13	04/10/93	20.21:48.3	61.94	1.44	2.3	1.0	11	5	EQ
14	07/11/93	23.40:44.0	67.84	20.08	2.5	1.7	15	4	EQ
15	07/11/93	23.43:17.2	66.28	7.02	3.1	2.5	25	4	EQ
16	08/11/93	14.28:17.3	59.91	2.72	2.4	1.5	15	7	EQ
17	12/11/93	19.54:36.0	59.69	12.86	3.4	2.9	16	6	EQ
18	15/11/93	15.04:25.6	62.17	3.27	2.7	1.9	15	5	EQ
19	21/11/93	01.53:56.3	60.18	4.96	2.6	2.1	12	6	EQ
20	27/11/93	18.57:52.7	60.47	11.66	3.1	2.2	0	5	EXP
21	13/12/93	09.00:09.5	56.75	2.74	3.1	2.6	12	6	EQ
22	27/12/93	05.20:46.3	61.29	2.79	3.3	3.6	14	8	EQ
23	03/01/94	22.12:59.8	61.76	4.19	2.6	2.4	17	7	EQ
24	07/01/94	09.06:22.6	60.60	2.43	2.3	1.8	23	5	EQ
25	15/01/94	00.00:26.2	65.23	7.58	2.8	1.6	2	3	EQ
26	19/01/94	09.16:54.8	66.36	14.60	2.4	1.4	0	3	EXP
27	21/01/94	01.26:14.1	65.98	11.89	3.1	2.1	19	2	EQ
28	25/01/94	03.07:58.3	62.46	5.07	2.6	1.9	20	5	EQ
29	26/01/94	17.27:47.1	66.84	13.58	3.0	2.3	0	5	EXP

ing magnitudes and moments for the 29 events listed in table I using the approach detailed in the previous section.

4.1. A_{max} *deduced from* A_{rms}

In figs. 2a-f to 4a-f the apparent validity of the A_{max}–A_{rms} relationship is demonstrated for station KMY recording of Event 4 in table I. In (a) the P and L_g phase recordings are shown; (b)-(c) the independently observed A_{max} versus A_{rms} or STA for both P and L_g waves; (d)-(e) the corresponding number of extremes within the individual STA windows. Note that an extrem occurs when the second derivative of the trace time function is zero. For unfiltered traces, as in figs. (d) and (e), the number of extreme would be relatively high due to the ripples overlaying the signal trace. The linear $A_{max} - A_{rms}$ relationship in

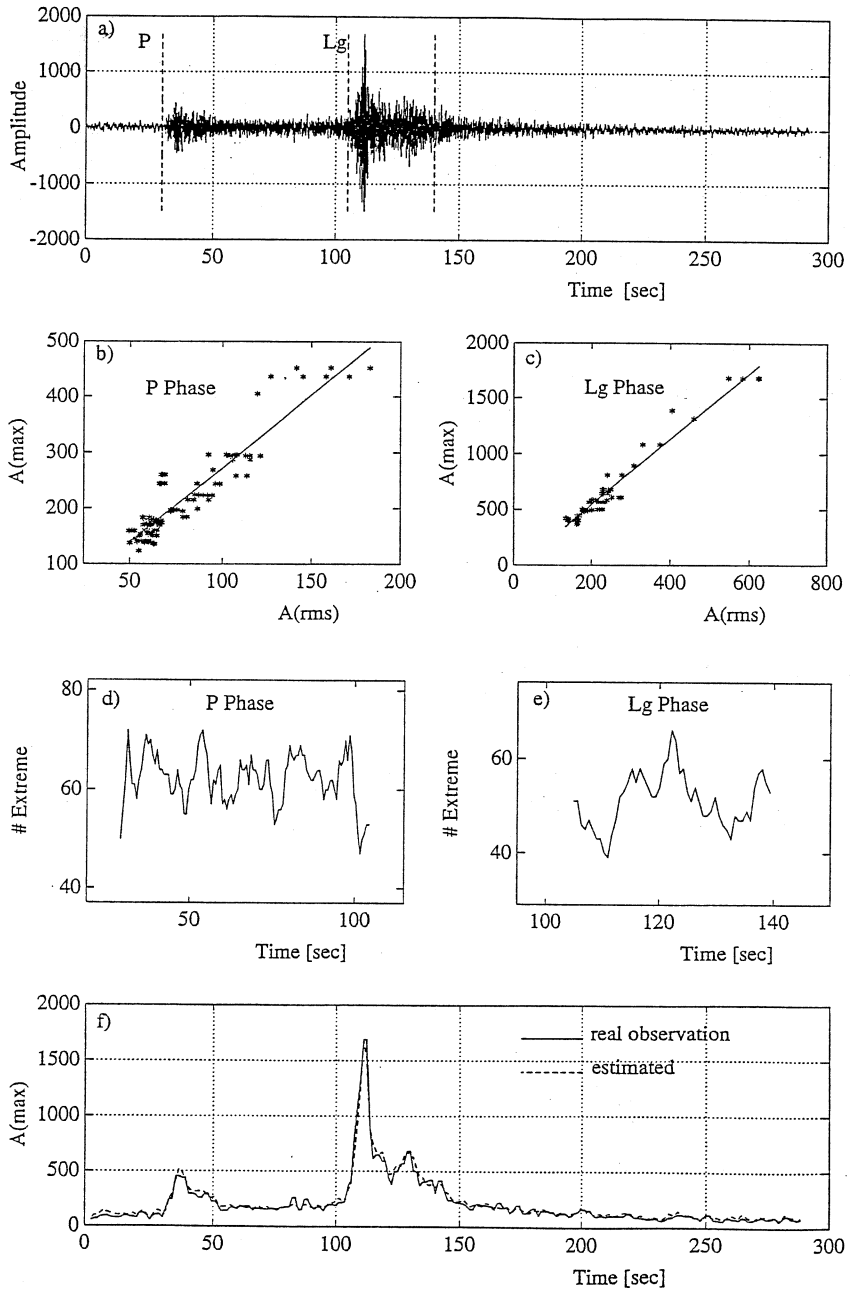

Fig. 2a-f. A_{max}–A_{rms} analysis for KMY unfiltered recordings of Event 4 in table II at an epicentral distance of 795 km. a) Original vertical trace record; b) and c) A_{max} versus A_{rms} for *P*- and L_g-phases respectively. The window length used in the evaluation of A_{rms} is 2.5 s; d) and e) number of extremes *N* for *P*- and L_g-phases; f) observed and estimated A_{max} using eq. (2.3). The two curves match each other almost perfectly.

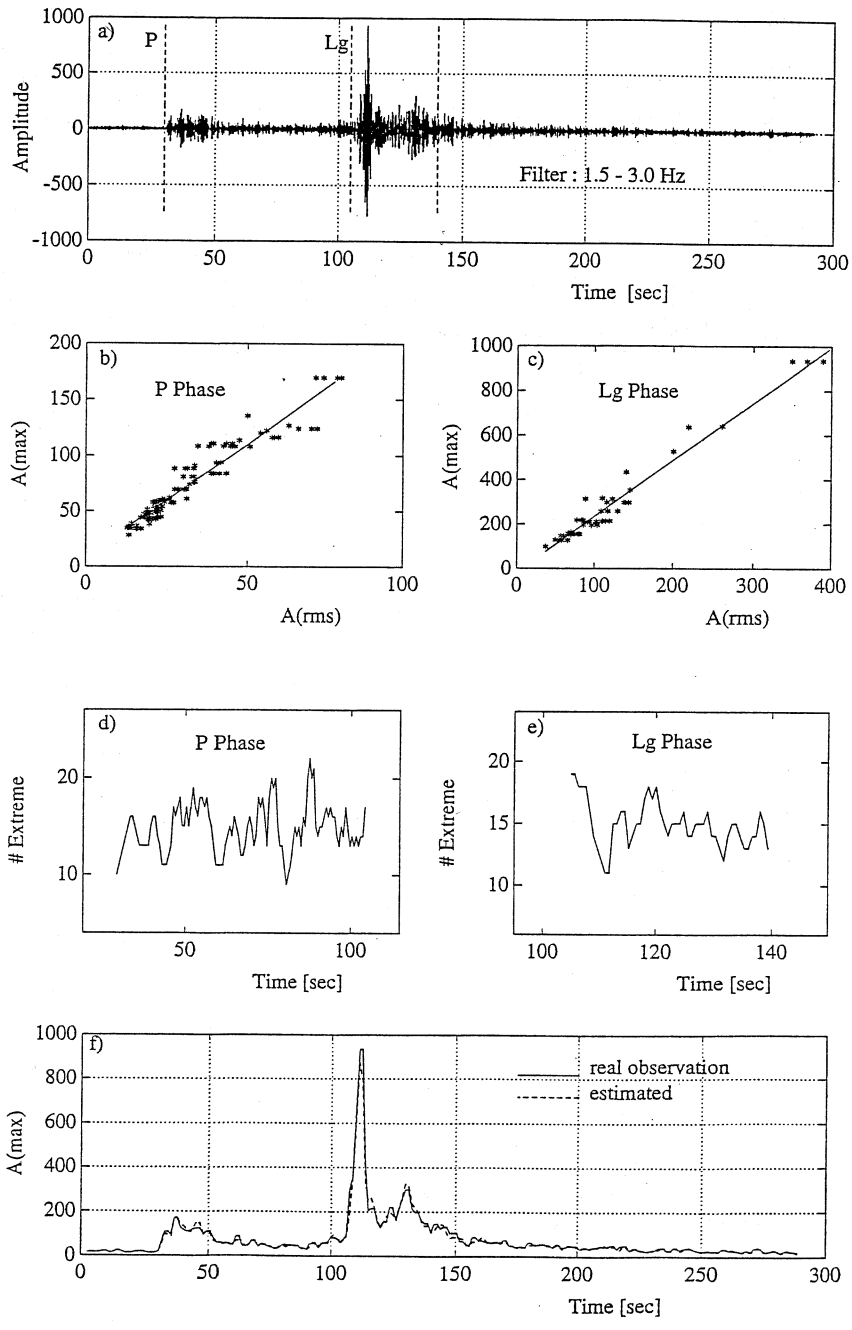

Fig. 3a-f. A_{max}–A_{rms} analysis for KMY recordings in the 1.5-3.0 Hz passband of Event 4 in table II. Otherwise, caption as in fig. 2a-f.

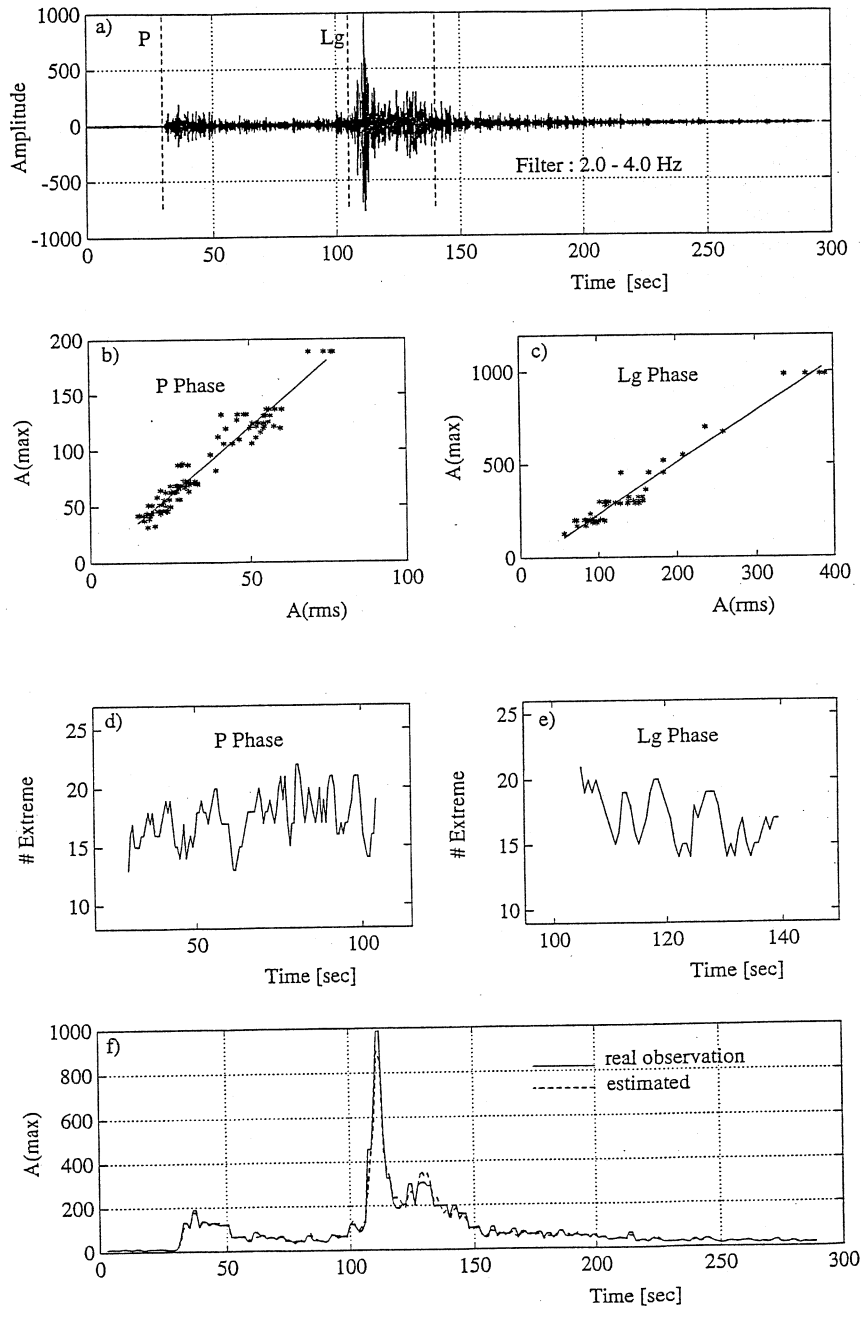

Fig. 4a-f. A_{max}–A_{rms} analysis for KMY recordings in the 2.0-4.0 Hz passband of Event 4 in table II. Otherwise, caption as in fig. 2a-f.

figs. (b) and (c) can be predicted from the number of extremes (N) in figs. (d) and (e); the agreement is very good. From this result we expect an excellent agreement between observed and estimated A_{max} values which indeed is the case from results presented in figs. (f). Even in the extreme cases of very peaked L_g-waves, this agreement remains good.

So far, we have computed the N-parameter for every STA window: since this parameter fluctuates moderately within a specific filter band and the $(2\ln N)^{1/2}$ expression of eq. (2.3) vary slowly with N, there is really no need to update the N-estimates for every STA window. Anyway, the essence of the results presented in figs. 2a-f to 4a-f is that the STA values as estimated in near real-time for a rms type of STA/LTA detector can be used for accurately estimating the maximum trace amplitudes for any part of the short period seismometer records.

4.2. *Magnitude estimation*

Given the epicentral distance and A_{max} or A_{rms}, we can compute event magnitudes or event moments as detailed above. This was done for the 29 events listed in table I and then these moments were converted to event magnitudes using the conversion formulas and the parameter values given in table III. These moment magnitudes are denoted $ML(\text{Ser})_{max}$ and $ML(\text{Ser})_{rms}$. Since frequency dependence on M_L-estimates is a debated topic, we computed ML(Ser) for 5 frequency bands as indicated in table II. Using the maximum amplitude values for S or L_g-phases we also computed conventional event magnitudes using various types of correction curves (spreading and attenuation) as taken from NORSAR, Alsaker *et al.* (1991), and the Seismological Observatory in Helsinki (details also in table III). In the latter cases, there is hardly any frequency dependence in the distance correction term, so here only the *f2* (1.5-3 Hz) frequency band was used in the magnitude calculations.

In table II all magnitude values represent averages with respect to the number of reporting stations listed in table I. The obtained event magnitudes are similar at the lower frequencies, irrespective of epicenter distance. The only exception here is the ML_H which are consistently high by ca. 0.6 magnitude units. A comparison with the coda magnitudes (M_c) gives that these are also consistently high and besides appear to be less stable than the NORSAR reference magnitudes (M_L). The latter are in reasonable agreement with the *f2* ML(Ser) values in table II that are consistently low by ca. 0.3 magnitude units. These features are illustrated in fig. 5a,b showing plots of $ML(\text{Ser})_{max}$ versus M_L-magnitudes reported by NORSAR.

Frequency dependence of the magnitude estimates is obvious from the table II results, but there is hardly any difference between the $ML(\text{Ser})_{rms}$ and $ML(\text{Ser})_{max}$ estimates. The attenuation parameter may be important in this respect, so we recalculated the ML(Ser) magnitudes for $\gamma = 0.20$ and $\gamma = 0.14$ equivalent to increased signal attenuation. Its effect is to increase the *f4* and *f5* magnitudes by only 0.1 magnitude units in average since epicenter distances are generally less than 250 km. On the other hand, the differences between *f1* and *f2* as compared to *f4* and *f5* magnitude estimates remain at ca. 0.4 magnitude units. In fig. 6a-f we have plotted event magnitudes for individual stations as a function of distance for $\gamma = 0.26$, $\gamma = 0.40$ and $\gamma = 0.55$ which are equivalent to decreasing attenuation. In these plots the average event magnitude is adjusted to a value of 2.5 units, while the stations at distances less than 250 km are deleted since the effect of frequency dependence is as mentioned very small for such ranges. From fig. 6a-f, we see that a γ value of 0.40 or 0.55 would be a better choice than $\gamma = 0.26$. These results contradicting those in table II, are not considered conclusive since we have few observations beyond 500 km and the scattering in the individual stations M_L values is of the order of some tens of a magnitude unit.

Table II. Magnitude estimates for the events listed in table I. $f1, f2, f3, f4$ and $f5$ represent different frequency bands which are 1-2 Hz, 1.5-3 Hz, 2-4 Hz, 3-6 Hz and 4-8 Hz, respectively. Column M_L is L_g event magnitudes as reported by NORSAR using NORESS recordings while M_c is coda magnitude based NSN recordings as reported in the bulletin. $ML(\text{Ser})_{\max}$ is magnitude estimates tied to maximum amplitude observations (eq. (3.8)) while $ML(\text{Ser})_{\text{rms}}$ are corresponding moment magnitude estimates tied to the rms values (eq. (3.7)). Common features are averaging over reporting stations (table I) and using Sereno *et al.* (1988) spreading and attenuation constants (table III). Columns ML_N, ML_A and ML_H are magnitude estimates similar to $ML(\text{Ser})_{\max}$ except that the distance correction terms used are those of NORSAR, Alsaker *et al.* (1991) and Helsinki (table III). Since these are frequency independent only magnitudes in the $f2$ band are listed. Note the overall similarity of event magnitudes in the $f2$ band with the exception of ML_H and M_c estimates. Another notable feature is the consistent decay in $ML(\text{Ser})$ from the $f1$-$f2$ bands towards the $f4$-$f5$ bands. We take this to imply that the S/L_g excitation is less effective at higher signal frequencies.

N.	M_L	M_c	$ML(\text{Ser})_{\max}$					$ML(\text{Ser})_{\text{rms}}$					ML_N	ML_A	ML_H
			$f1$	$f2$	$f3$	$f4$	$f5$	$f1$	$f2$	$f3$	$f4$	$f5$	$f2$	$f2$	$f2$
1	2.2	2.6	2.5	2.3	2.2	2.0	2.0	2.6	2.4	2.3	2.1	2.1	2.3	2.3	2.9
2	2.5	2.8	2.9	2.8	2.7	2.6	2.5	3.0	2.9	2.8	2.6	2.5	2.8	2.7	3.3
3	2.0	2.7	2.5	2.3	2.2	2.1	2.0	2.6	2.5	2.4	2.2	2.1	2.3	2.3	2.9
4	3.2	3.9	3.7	3.7	3.6	3.5	3.5	3.7	3.6	3.5	3.2	2.9	3.8	3.6	4.1
5	1.6	2.1	2.1	1.9	1.8	1.6	1.5	2.2	2.0	1.9	1.7	1.6	1.8	1.8	2.4
6	1.8	3.2	2.0	1.8	1.9	2.3	2.3	2.1	1.9	2.0	2.3	2.3	1.9	1.9	2.4
7	2.5	3.0	2.7	2.6	2.5	2.5	2.4	2.8	2.7	2.6	2.5	2.4	2.6	2.5	3.1
8	2.3	2.9	2.3	2.2	2.3	2.3	2.1	2.4	2.3	2.3	2.2	1.8	2.2	2.2	2.8
9	1.4	1.6	1.6	1.4	1.3	1.1	0.9	1.8	1.5	1.4	1.2	1.1	1.3	1.3	1.8
10	2.2	2.8	2.5	2.4	2.3	2.1	2.0	2.7	2.5	2.4	2.2	2.0	2.4	2.4	3.0
11	1.5	1.8	1.8	1.5	1.3	1.2	1.1	1.9	1.7	1.5	1.4	1.2	1.3	1.4	2.0
12	1.8	2.5	2.1	2.0	1.9	1.8	1.7	2.2	2.1	2.0	1.9	1.7	1.8	1.9	2.5
13	1.0	2.3	1.8	1.5	1.5	1.4	1.3	1.9	1.6	1.5	1.3	1.2	1.5	1.5	2.0
14	1.7	2.5	2.3	2.2	2.1	1.8	1.6	2.4	2.3	2.1	1.8	1.5	2.1	2.1	2.7
15	2.5	3.1	2.9	2.9	2.8	2.5	2.5	3.0	2.9	2.7	2.4	2.2	2.9	2.8	3.5
16	1.5	2.4	2.1	1.8	1.7	1.6	1.5	2.1	1.8	1.7	1.6	1.5	1.7	1.7	2.3
17	2.9	3.4	3.1	2.9	2.9	2.8	2.7	3.2	3.0	2.8	2.6	2.3	3.0	2.9	3.5
18	1.9	2.7	2.4	2.3	2.2	2.1	2.0	2.5	2.3	2.3	2.1	1.9	2.2	2.2	2.8
19	2.1	2.6	2.4	2.3	2.2	1.9	1.8	2.4	2.3	2.3	2.1	1.9	2.1	2.1	2.7
20	2.2	3.1	2.6	2.5	2.3	2.2	2.1	2.7	2.6	2.4	2.1	1.9	2.5	2.5	3.1
21	2.6	3.1	2.4	2.3	2.3	2.4	2.4	2.5	2.3	2.3	2.2	2.0	2.3	2.3	2.9
22	3.6	3.3	3.6	3.4	3.2	3.0	2.9	3.7	3.4	3.2	2.9	2.7	3.4	3.3	3.9
23	2.4	2.6	2.9	2.7	2.7	2.5	2.4	2.9	2.8	2.7	2.5	2.4	2.6	2.6	3.3
24	1.8	2.3	2.2	2.1	2.0	1.8	1.7	2.3	2.1	2.0	1.8	1.7	2.0	2.0	2.6
25	1.6	2.8	2.0	1.8	1.8	1.9	1.9	2.1	1.9	1.9	1.8	1.7	1.8	1.8	2.4
26	1.4	2.4	2.0	1.7	1.5	1.3	1.3	2.1	1.8	1.5	1.4	1.4	1.7	1.7	2.2
27	2.1	3.1	2.4	2.3	2.2	2.1	2.0	2.5	2.4	2.3	2.2	2.1	2.2	2.2	2.9
28	1.9	2.6	2.3	2.0	1.9	1.7	1.6	2.3	2.1	1.9	1.7	1.5	1.9	1.9	2.5
29	2.3	3.0	2.4	2.3	2.2	2.1	1.9	2.5	2.4	2.3	2.1	1.9	2.2	2.2	2.8

The above attenuation results signify the importance of path effects and station corrections, and also the observational fact that L_g-wave excitation is relatively less effective at signal frequencies above 3-4 Hz.

5. Discussion

In this study we have explored the possibility of estimating event magnitude in near real time. At this stage of development we have concentrated on demonstrating that

Table III. Listing of correction formulas as used for the estimated magnitudes tabulated in table II. M_0 = moment, A = peak amplitude in nm and Δ = epicentral distance in km. $F(\Delta, T)$ correction function is shown in fig. 7 for T = 0.45 s.

Magnitude formulations	Reference
$\log M_0 = 1.03\ ML(\text{Ser}) - 17.1$ (EQ) $\log M_0 = 1.04\ ML(\text{Ser}) - 17.7$ (EXP) $Q_0 = 560;\ \gamma = 0.26$ $r_0 = 100$ km; $\mu = 1;\ \nu = 1/2$ $\varrho = 2.7$ gr/cm^3; $\beta = 3.5$ km/s	Sereno *et al.* (1989)
$ML_N = \log(100\,A) + F(\Delta, T)$	NORSAR
$ML_A = \log A + 0.91 \log \Delta + 0.00087\,\Delta - 1.31$	Alsaker *et al.* (1991)
$ML_H = \log A + 1.27 \log \Delta - 1.44$	Helsinki Seismological Observatory

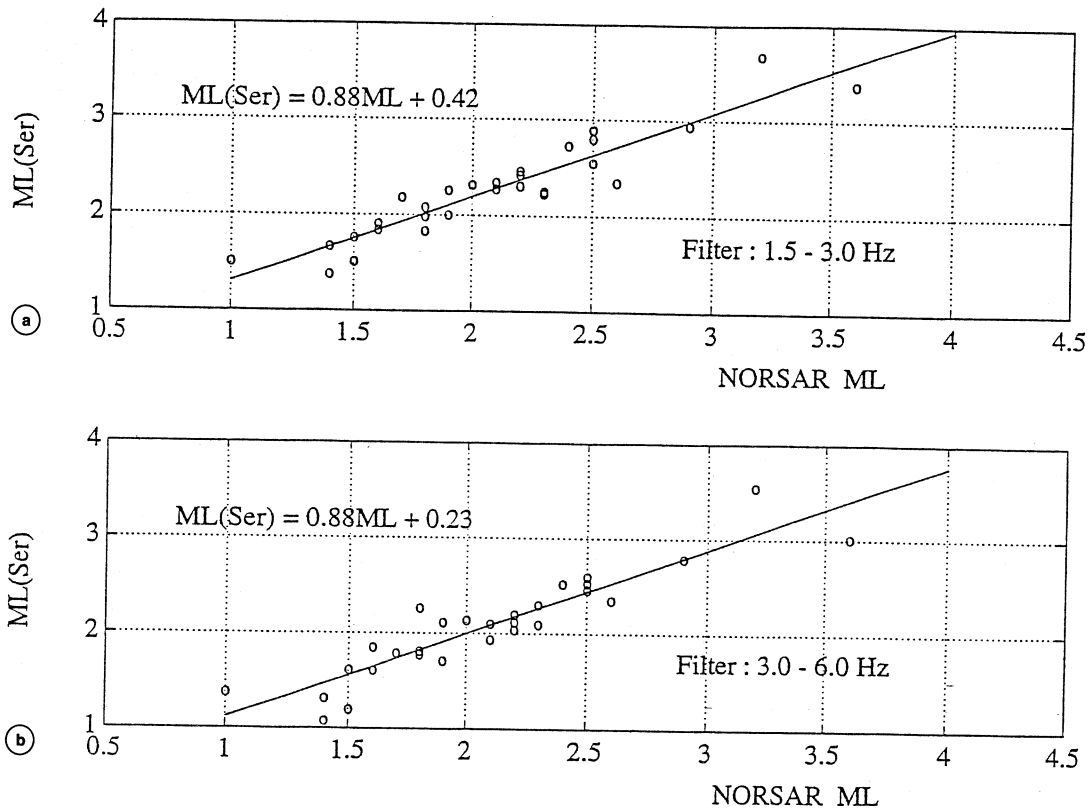

Fig. 5a,b. $ML(\text{Ser})_{\max}$ magnitude estimates from table II versus the reference NORSAR M_L magnitude estimates in table II. The small offset may in part reflect local site effects since the NORESS array is located outside the NSN siting area.

A_{max} and/or A_{rms} and hence event magnitudes can be obtained from signal detector outputs of the STA/LTA types. In figs. 2a-f to 4a-f, an excellent agreement between observed and estimated maximum amplitude in all frequency bands considered is demonstrated. However, we have not contemplated such maximum amplitude estimates in a real time operational environment since we are not directly involved in this kind of work.

Through the analysis of 29 events (earthquakes and explosions) we have determined A_{max} and A_{rms} as described above for both conventional and moment magnitude estimates. In the former cases, we used empirical formulas for the geometrical spreading and attenuation effects taken from Alsaker *et al.* (1991) and those used at NORSAR and Helsinki in their bulletin works. In many regions such correction tables are not available, so we explored the possibility of using moment magnitudes based on spreading and attenuation parameters estimated directly from spectral analysis of local event records. All the various types of M_L estimates for local events recorded by the Norwegian Seismograph Network (NSN) stations proved to be mutually consistent. The only exception here was the *ML* Helsinki estimates which appeared to be positive biased by ca. 0.6 magnitude units. In the NSN monthly bulletins, coda magnitudes are routinely reported. These estimates also appear to be positive biased and somewhat unstable.

Initially, we allowed the corner frequency (f_c) to be a free parameter but for larger events $M_L > 3.0$, this caused erroneous estimates in the sense that unrealistic magnitudes estimates were obtained. The remedy here was to freeze the corner frequency at 20 Hz. This also implies that the estimate of the f_c parameter is not well constrained in the analysis procedure used. For larger events, say for $M_L > 4.5$, some of the frequency bands considered here would be beyond the corner frequency and hence the corresponding moment magnitude estimates should have negative biases. Indications of such cases would be negative differences between low and high frequency bands, actually observed for nearly all events used in analysis (table II). From the previous section, we rule out relatively strong signal attenuation or exceptionally low corner frequencies as a plausible explanation for these observational features. Instead, we consider that the S/L_g signal excitation spectra are not flat met to the corner frequency as presumed in our theoretical modelling. In other words, the most consistent and correct magnitude estimates are obtained for signal frequencies in 1-3 Hz range; at higher signal frequencies the observed negative biases can be computed by introducing frequency dependent station corrections if considered worth while.

A recent tendency in establishing local magnitude scales is the synthesis of the original Wood-Anderson seismograph recordings from Southern California (Richter, 1935) (*e.g.* Alsaker *et al.*, 1991). Our preference is for the moment magnitude estimation approach simply because of its anchoring on physical source representation and well established wave propagation parameters. These parameters can be obtained through analysis of appropriate signal spectra (Sereno *et al.*, 1988) which besides would be representative of the station/network siting area. In contrast, the wave propagation regime of Southern California is not representative for most of the network areas elsewhere and hence not well suited as a magnitude reference base. In a seismic hazard study for Southern Norway, Singh *et al.* (1990) discussed various magnitude formulas in use and also the associated attenuation parameters including those of Sereno *et al.* (1988). The differences here appear larger than the corresponding differences in estimated event magnitudes and a reconciling explanation here is that spreading and attenuation effects are not easily separated. The combined effects are incorporated in the magnitude correction curves. The relative consistency of *ML*(Ser) magnitudes (table II) implies that it should be possible to construct

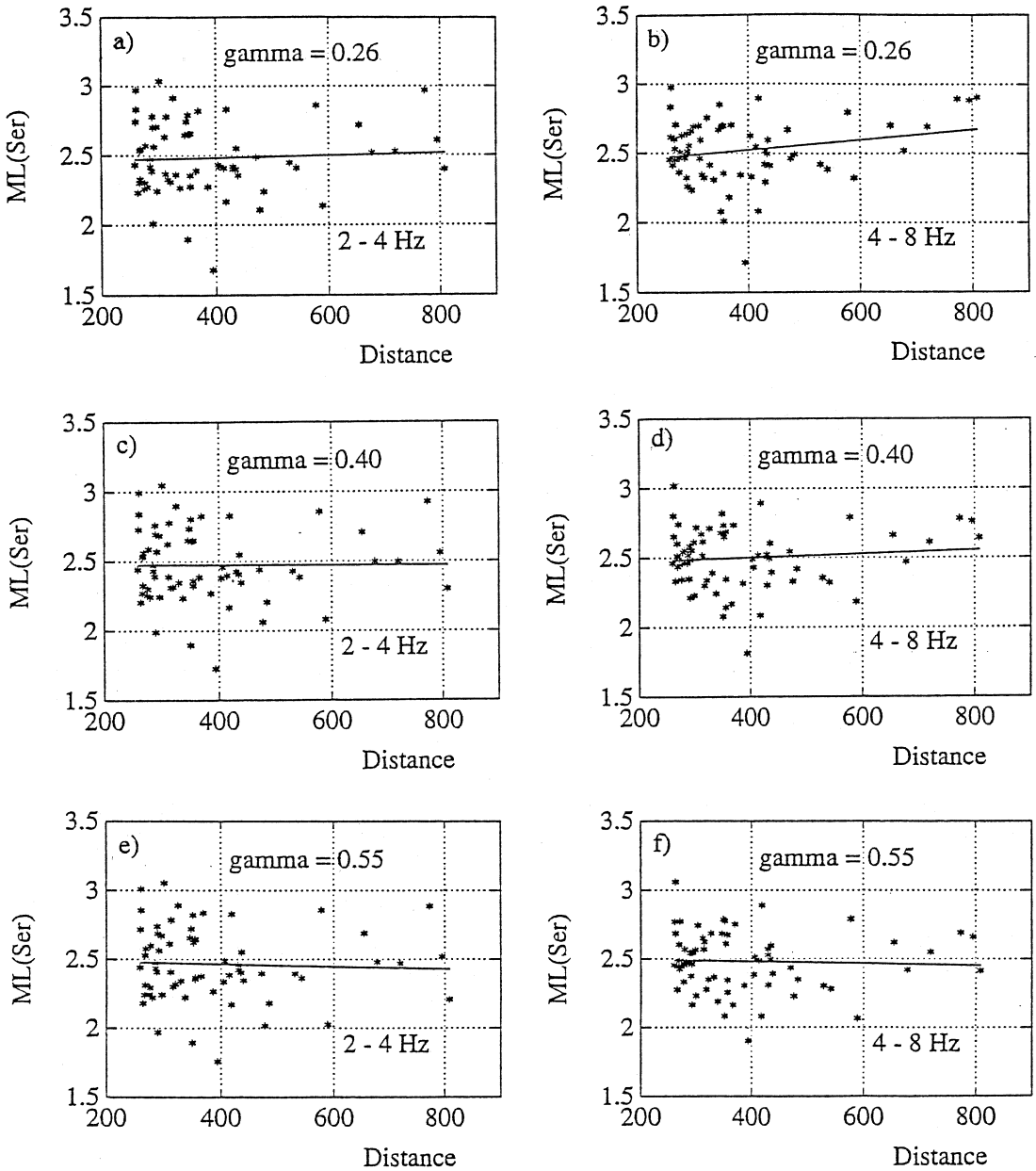

Fig. 6a-f. The ML(Ser) estimates as a function of epicenter distance and different values of the attenuation parameter γ. The corresponding linear regression lines are also shown. Note that network $ML(\mathrm{Ser})_{\max}$ average for each event is scaled to a reference magnitude of 2.5 units and this scaling constant would be different for each frequency band considered. Observations for distances below 250 km were excluded from the figure. There are very few observations beyond 500 km so it is not quite obvious that the best fitting $\gamma = 0.40$ (diminishing attenuation) is truly correct. The table II results give less differences between low and high frequency estimates for the decreasing γ values.

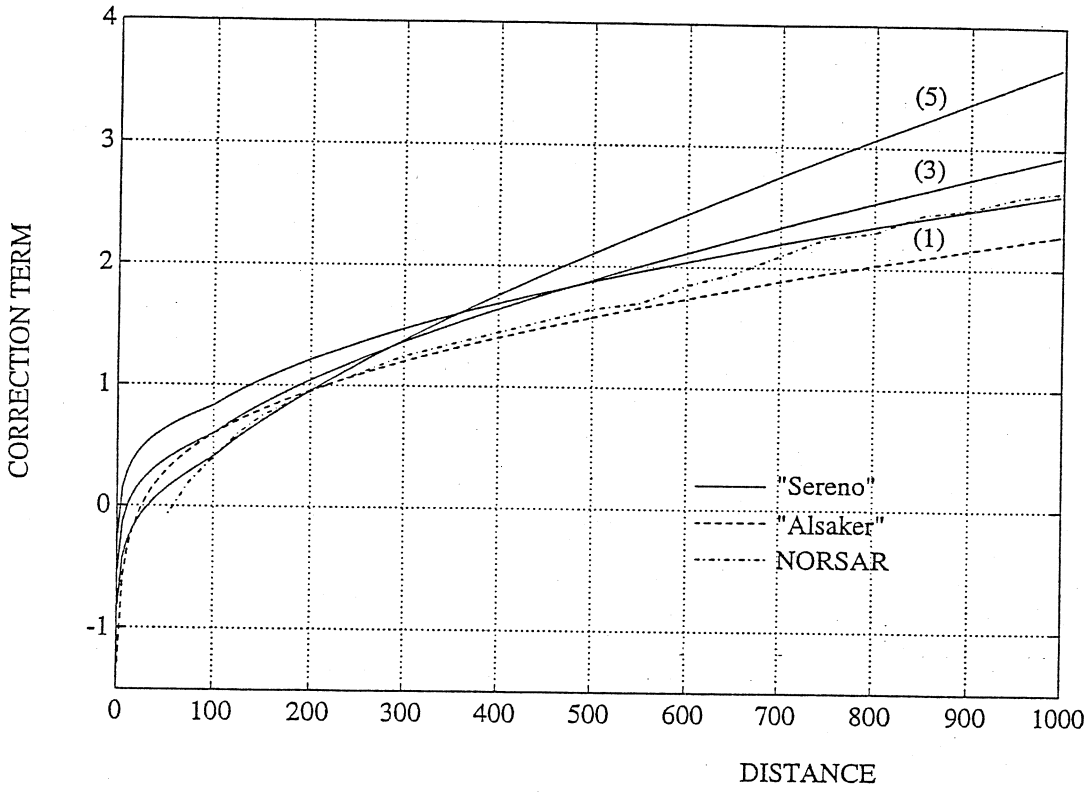

Fig. 7. Generating distance-correction curves from the Sereno *et al.* (1988) spreading and attenuation parameters as listed in table III. For comparison the corresponding Alsaker *et al.* (1991) and NORSAR (T = 0.45 s) curve are shown. The correction curves derived from Sereno *et al.* (1988) are plotted for the filters $f1$, $f3$ and $f5$. In table II the ML(Ser) and ML_A magnitude estimates are very similar which is also expected from fig. 7 since epicenter distances generally are less than 250 km. The NORSAR reported magnitudes (M_L column in table II) are in average 0.3 units lower than expected since the corresponding epicenter distances are in the 300-600 km range. Note that the different correction curves are similar out to ca. 350 km that is the distance range where the majority of local events are recorded.

correction tables, the $q(r, f)$-term in eq. (1.1), from the spreading and attenuation parameters in eq. (3.9). Such correction curves are shown in fig. 7 for the center frequencies and bandwidths of the bandpass filters used and the Alsaker *et al.* (1991) and NORSAR correction curves are included for comparison. In table II the ML_A magnitudes are very similar to the ML(Ser) ones as expected from fig. 7 since the epicenter distances seldom exceed 250 km. Likewise, the NORSAR reported M_L magnitudes are in average 0.3 units below the ML(Ser) ones. This is also easily explained from fig. 7 since the NORSAR epicenter distances (see fig. 1) are mostly in the 300-600 km range where the associated correction curve is lower by ca. 0.3 units. In other words, our magnitude estimates and distance corrections pertain to epicenter dis-

tances well below 500 km. Ruud and Husebye (1992) have demonstrated that at least in Fennoscandia most of the station event recordings pertain to epicenter distances less than 500 km. If magnitude is to be retained as a standard earthquake size measure, a universal moment to magnitude formula may be constituted say by IASPEI, in order to avoid the prevailing confusion on type of event magnitude as published for local and regional events. A final remark is that near real time event magnitude estimates would be invaluable for estimating network monitoring capabilities also in near real time. Such estimates are tied to noise level estimates from the individual network stations in combination with a grid search procedure (*e.g.* Sereno and Bratt, 1989; Ringdal and Kværna, 1992). Another application now under consideration is to use near real time magnitude estimates as a part of automated epicenter location schemes (Ruud *et al.*, 1993; Sambridge and Gallanger, 1993) that is by incorporating both phase and amplitude consistency in the phase association routine and hence in the final epicenter location.

6. Concluding remarks

In this study we have demonstrated that near real time magnitude estimation is feasible conditioned on a signal detector design for determining peak signal trace amplitudes. The results presented in table II imply that moment magnitudes are a viable alternative to conventional magnitude estimates. The advantages are an anchoring to seismic source theory and the use of clearly defined signal spreading and attenuation parameters. We have also demonstrated that the spreading and the attenuation parameters can be used for construction of correction tables commonly used in conventional magnitude determinations, thus avoiding tedious analysis of many earthquake recordings (Alsaker *et al.*, 1991).

Acknowledgements

Stimulating discussions with Bent Ole Ruud (Bergen University) and Dr. Anton Dainty (Philips Laboratory, Hanscom AFB, Ma) are hereby acknowledged. The research was supported by the Air Force Office of Scientific Research, USAF under Grant F49620-92-J-0510 (E.S.H.). TÜBİTAK (Marmara Research Center) is thanked for providing the opportunity to participate in this work, while financial support from the Norwegian Research Council (NFR) is much appreciated (C.D.M.).

REFERENCES

AKI, K. (1967): Scaling law of seismic spectrums, *J. Geophys. Res.*, **73**, 1217-1231.

ALSAKER, A., L.B. KVAMME, R.A. HANSEN, A. DAHLE and H. BUNGUM (1991): The M_L scale in Norway, *Bull. Seismol. Soc. Am.*, **81**, 379-398.

BOORE, D.M. (1983): Stochastic simulation of high-frequency ground motions based on seismological models of the radiated spectra, *Bull. Seismol. Soc. Am.*, **73**, 1865-1894.

BOORE, D.M. and W.B. JOYNER (1984): A note on the use of random vibration theory to predict peak amplitudes of transient signals, *Bull. Seismol. Soc. Am.*, **74**, 2035-2039.

BÅTH, M. (1981): Local magnitude: recent research and current trends, *Earth Sci. Rev.*, **17**, 315-398.

CARTWRIGHT, D.E. and M.S. LONGUET-HIGGINS (1956): The statistical distribution of the maxima of a random function, *Proc. Roy. Soc. London, Ser.* **A237**, 212-223.

CRANDAL, S.H. and W.D. MARK (1963): Random Vibration in Mechanical Systems (Academic Press, New York and London).

DZIEWONSKI, A.M. and F. GILBERT (1974): Temporal variation of the seismic moment tensor and the evidence of precursive compression for two deep earthquakes, *Nature*, **247**, 185-188.

EBEL, J.E. (1982): M_L measurements for Northeastern United States earthquakes, *Bull. Seismol. Soc. Am.*, **72**, 1367-1378.

JOST, M.L. and R.B. HERRMANN (1989): A student's guide to and review of Moment Tensors, *Seismol. Res. Lett.*, **60** (2), 37-57.

NUTTLI, O.W. (1973): Seismic wave attenuation and magnitude relations for Eastern North America, *J. Geophys. Res.*, **78**, 876-885.

RICHTER, C.F. (1935): An instrumental earthquake magnitude scale, *Bull. Seismol. Soc. Am.*, **25**, 1-32.

RINGDAL, F. and T. KVÆRNA (1992): Continuous seismic threshold monitoring, *Geophys. J. Int.*, **111**, 505-514.

RUUD, B.O. and E.S. HUSEBYE (1992): A new three-component detector and automatic single station bulletin production, *Bull. Seismol. Soc. Am.*, **82**, 221-237.

RUUD, B.O., C.D. LINDHOLM and E.S. HUSEBYE (1993): An exercise in automating seismic record analysis and network bulletin production, *Bull. Seismol. Soc. Am.*, **83**, 660-679.

SAMBRIDGE, M. and K. GALLAGHER (1993): Earthquake hypocenter location using genetic algorithms, *Bull. Seismol. Soc. Am.*, **83**, 1467-1491.

SERENO, T.J., S.R. BRATT and T.C. BACHE (1988): Simultaneous inversion of regional wave spectra for attenuation and seismic moment in Scandinavia, *J. Geophys. Res.*, **93**, 2019-2035.

SERENO, T.J. and S.R. BRATT (1989): Seismic detection capability at NORESS and implications for the detection threshold of a hypothetical network in the Soviet Union, *J. Geophys. Res.*, **94**, 10397-10414.

SINGH, S.K., M. ORDAZ, C.D. LINDHOLM and J. HAVSKOV (1990): Seismic hazard in Southern Norway, *Tech. Rep.* Seismo-series N. 46, University of Bergen, Norway.

XIE, J. (1993): Simultaneous inversion for source spectrum and path Q using L_g with application to three semipalatinsk explosions, *Bull. Seismol. Soc. Am.*, **83**, 1547-1562.

Appendix

The relation between A_{rms} and $|A(f, r)|$:

Rayleigh's theorem gives the energy relation between the time and frequency domain representations such as:

$$\int_{-\infty}^{\infty} |\, a(t)\,|^2 dt = \int_{-\infty}^{\infty} |\, A(f)\,|^2 df \tag{A.1}$$

where $a(t)$ is the displacement in time and $|A(f)|$ is the amplitude spectrum. The unbiased rms estimate of the signal $a(t)$ in continuous time is defined as:

$$A_{\text{rms}}^2 = \frac{1}{\Delta T} \int_0^{\Delta T} |\, a(t)\,|^2 dt \tag{A.2}$$

where ΔT is window length in s. Likewise, for digital signals we have

$$A_{\text{rms}}^2 = \frac{1}{N} \sum_{i=0}^{N-1} a_i^2 \tag{A.3}$$

where N is the number of the samples. From eq. (3.1), we assume that $|\, A(f, r)\,|$ is flat within the passband of the filters used and this in combination with the Rayleigh's theorem leads to:

$$\begin{aligned} A_{\text{rms}}^2 &= \frac{1}{\Delta T} \int_{-f_B}^{f_B} |\, A(f)\,|^2 df \\ &= \frac{1}{\Delta T} \left[\int_{-f_2}^{-f_1} |\, A(f)\,|^2 df + \int_{f_1}^{f_2} |\, A(f)\,|^2 df \right] \\ &= \frac{1}{\Delta T}\, 2\Delta f\, |\, A(f_0)|^2 \end{aligned} \tag{A.4}$$

where f_B is the bandwidth of $a(t)$, f_1 and f_2 are the low and high cutoff frequencies of the bandpass filter, Δf is the filter bandwidth ($\Delta f = f_2 - f_1$) and f_0 is the center frequency [$f_0 = (f_1 + f_2)/2$] of the bandpass filter. Thus, eq. (A.4) gives us the relationship between the rms value of the signal $a(t)$ and the amplitude of the spectrum at the frequency f_0 which is expressed as:

$$| A(f_{0i}, r) | = \sqrt{\frac{\Delta T}{2\Delta f_t}} A_{\text{rms}}; \quad i = 1, ..., 5 \tag{A.5}$$

where f_{0i} and Δf_i are the center frequencies and the bandwidths of the 5 bandpass filters used in data analysis, $|A(f_{0i}, r)|$ is the amplitude spectrum of the displacement at epicentral distance r. In data analysis ΔT being the STA window length is fixed at 5 s independent of the bandpass filter used. In the context of detector design the STA window lengths seldom exceed a few seconds, however it is easy to combine short STA(rms) values in order to produce longer rms.

The relation between A_{max} and $|A(f, r)|$:

Assuming that the amplitude spectrum of the displacement $a(t)$ is flat within an idealized bandpass filtered trace, we have:

$$| A(f)| = A_0\Pi_{\Delta f}(f - f_0) + A_0\Pi_{\Delta f}(f + f_0) \tag{A.6}$$

where $\Pi_{\Delta f}$ is a rectangular function with unit amplitude and bandwidth Δf, f_0 is the center frequency of $\Pi_{\Delta f}$ and A_0 is the amplitude of the displacement spectrum. If $A(f)$ is a real function, its inverse Fourier transform is:

$$a(t) = 2\Delta f A_0 \text{sinc}(\Delta f t)\cos(2\pi f_0 t) \tag{A.7}$$

$a(t)$ has a maximum value at $t = 0$, namely

$$\begin{aligned} A_{\text{max}} &= 2\Delta f A_0 \\ &= 2\Delta f \, | A(f_{0i}, r) |; \quad i = 1 ,..., 5 \end{aligned} \tag{A.8}$$

Eq. (A.7) is only valid in case of real functions (no phase shifts) which is hardly the case in seismology. However, since the *sinc* function varies rather slowly as compared to the *cos* function in eq. (A.7), it can be shown that the A_{max} relation in eq. (A.8) remains valid for practical purposes also for non-real functions.